Maleimidyl magnetic nanoplatform for facile molecular MRI

2014 Nanotechnology 25 275102

(http://iopscience.iop.org/0957-4484/25/27/275102)

IOP Publishing Nanotechnology
Nanotechnology **25** (2014) 275102 (10pp) doi:10.1088/0957-4484/25/27/275102

Maleimidyl magnetic nanoplatform for facile molecular MRI

Dan Heo[1,2,8], Eugene Lee[1,2,8], Minhee Ku[1,3], Seungyeon Hwang[1,2], Bongjune Kim[4], Yeonji Park[1], Young Han Lee[1], Yong-Min Huh[1,2,5,6], Seungjoo Haam[2,4], Jae-Ho Cheong[5], Jaemoon Yang[1,5] and Jin-Suck Suh[1,2,5,6]

[1] Department of Radiology, Yonsei University College of Medicine, Seoul, 120-752, Republic of Korea
[2] Nanomedical National Core Research Center, Yonsei University, Seoul, 120-749, Republic of Korea
[3] Brain Korea 21 plus Project for Medical Science, Yonsei University, Seoul, 120-752, Republic of Korea
[4] Department of Chemical and Biomolecular Engineering, Yonsei University, Seoul, 120-749, Republic of Korea
[5] YUHS-KRIBB Medical Convergence Research Institute, Seoul, 120-752, Republic of Korea
[6] Severance Biomedical Science Institute (SBSI), Seoul, 120-752, Republic of Korea
[7] Department of Surgery, Yonsei University, Seoul, 120-752, Republic of Korea

E-mail: 177hum@yuhs.ac (J Yang) and jss@yuhs.ac (J-S Suh)

Received 23 January 2014, revised 21 April 2014
Accepted for publication 7 May 2014
Published 24 June 2014

Abstract

In this study, we developed the maleimidyl magnetic nanoplatform, which enables functional targeting of a biomarker-specific moiety for molecular imaging via MRI. The maleimide group of the maleimidyl magnetic nanoplatform is conjugated with a thiol group without additional crosslinkers and side products. A physicochemical analysis was conducted to verify the effectiveness of the maleimidyl magnetic nanoplatform, and the existence of the maleimidyl group was investigated using the platform. To prepare biomarker-specific MRI probes, a thiolated aptamer and peptide were immobilized onto the maleimidyl group of the maleimidyl magnetic nanoplatform. The fabricated MRI probes were applied to four cancer cell lines: HT1080, MCF7, MKN45, and HEK293T. To investigate the potential of the molecular MRI probe, the target-biomarker specificity was confirmed without serious cytotoxicity, and *in vivo* MRI analysis using a xenograft mouse model was demonstrated. We believe these results will be useful for fabricating molecular MRI probes for the diagnosis of cancer.

S Online supplementary data available from stacks.iop.org/NANO/25/275102/mmedia

Keywords: maleimidyl, magnetic nanoplatform, magnetic resonance imaging, cancer, molecular imaging

(Some figures may appear in colour only in the online journal)

Abbreviations

MRI	magnetic resonance imaging
MNC	magnetic nanocrystal
mP80	maleimidyl polysorbate 80
EpCAM	epithelial cell adhesion molecules
MT1-MMP	membrane type-1 matrix metalloproteinase
P80	polysorbate 80
PCR	polymerase chain reaction
MPA	3-maleimidopropionic acid
MWCO	molecular weight cut off
PBS	phosphate-buffered saline
MNP	magnetite nanoparticle

[8] These authors contributed equally to this work.

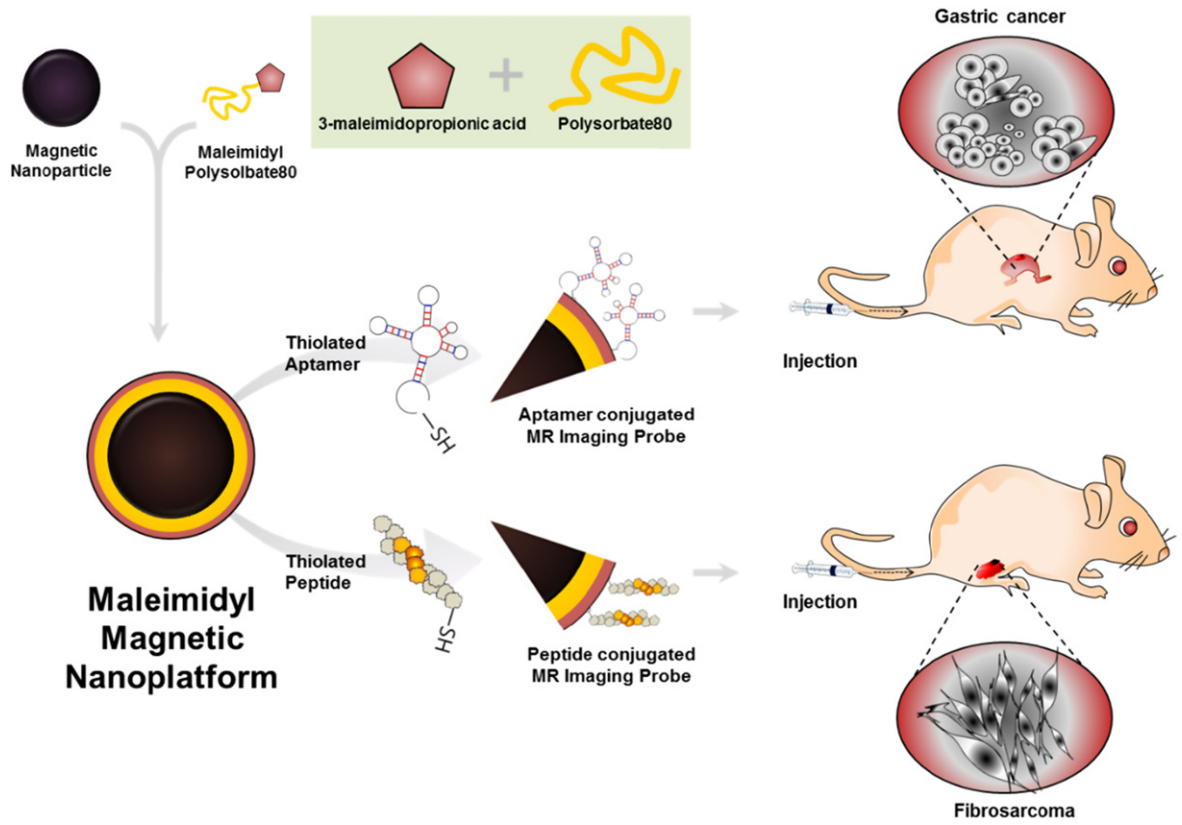

Figure 1. Schematic illustration of the preparation steps for biomarker-targetable magnetic nanoprobe for facile molecular MRI.

MFNP	manganese ferrite nanoparticle
mMNP	maleimidyl magnetite nanoparticle
mMFNP	maleimidyl manganese ferrite nanoparticle
pMNP	polysorbate 80-enveloped magnetite nanoparticle
pMFNP	polysorbate 80-enveloped manganese ferrite nanoparticle
P-mMNP	peptide-conjugated maleimidyl magnetite nanoparticle
P-mMFNP	peptide-conjugated maleimidyl manganese ferrite nanoparticle
A-mMFNP	aptamer-conjugated maleimidyl manganese ferrite nanoparticle
RNA	Ribonucleic acid
cDNA	complementary deoxyribonucleic acid
FITC	fluorescein isothiocyanate
FBS	fetal bovine serum
T2	transverse relaxation time
TE	echo time
TR	repetition time
H&E	hematoxylin and eosin
R2	relaxivity of transverse relaxation time
FT-IR	Fourier-transform infrared spectroscopy

1. Introduction

Magnetic resonance imaging (MRI) is a superior molecular imaging technique for the clinical diagnosis of cancer because of its noninvasive tomographic imaging and high spatial resolution [1, 2]. The sensitivity of MRI has been significantly improved in recent years using magnetic nanocrystals (MNCs) because an enhanced T2-shortening effect is ascribed to the high crystallinity of MNCs [3–5]. In particular, the immobilization of a targeting moiety on the MNC has facilitated biomarker-specific molecular MRI [6]. Thus, biomarker-specific molecular imaging enables the early and specific detection of cancer cells and facilitates the analysis of disease progression to improve survival rate [7, 8].

However, the existing immobilization methods using MNCs and targeting moieties need additional processes, such as the addition of crosslinkers or catalysts and purification to remove residual additives and side products. These additional processes may cause an increase in reaction time, low yield, contamination, and deterioration, which means a decline of economic feasibility.

To solve this problem, we developed a maleimidyl magnetic nanoplatform based on maleimide-functionalized polysorbate 80 (mP80). The mP80 is used not only to envelop magnetic nanoparticles for dissolving in water, but also to create linkages between magnetic nanoparticles and thiolated targeting moieties. The process of targeting-moiety conjugation using the maleimidyl magnetic nanoplatform is very economical because the side product does not appear and the

additional crosslinkers, or the process of removing residual additives, is not necessary for the reaction between the maleimide group and the thiol group. Therefore, the maleimidyl magnetic nanoplatform is functionalized simply by the thiolated targeting moieties for molecular MRI (figure 1).

In this study, we applied the maleimidyl magnetic nanoplatform to fabricate molecular MRI probes by combining monodispersed MNCs, mP80, and two targeting moieties of metastatic cancer biomarkers: epithelial cell adhesion molecules (EpCAM) and membrane type-1 matrix metalloproteinases (MT1-MMP) [9–12]. We conducted a physicochemical analysis to verify the effectiveness of the maleimidyl magnetic nanoplatform, and using this platform, we investigated the existence of the maleimidyl group. We investigated the targeted MRI potential of the fabricated MRI probes using various microscopic analyses and *in vitro* MRI of HT1080 and MKN45 cells. We also verified the *in vivo* targeting ability using a mouse xenograft model.

2. Materials and methods

2.1. Materials

Iron(III) acetylacetonate, manganese(II) acetylacetonate, 1,2-hexadecanediol, dodecanoic acid, dodecylamine, benzyl ether, polysorbate 80 (P80), 4-(dimethylamino)pyridine, N, N′-Dicyclohexylcarbodiimide, triethylamine, and dichloromethane anhydrous were purchased from Sigma Aldrich Chemical Co. (USA) and 3-maleimidopropionic acid (MPA) was purchased from TCI America (USA). The thiolated MT1-MMP-specific binding peptide (sequence: G-P-L-P-L-R-S-W-G-L-K-C) and the EpCAM aptamer (sequence: 5′-AGC GTC GAA TAC CAC TAC AGA GGT TGC GTC TGT CCC ACG TTG TCA TGG GGG GTT GGC CTG CTA ATG GAGC TCG TGG TCA G-3′) were purchased from PEPTRON (Republic of Korea) and Aptamer Science (Republic of Korea), respectively. Phosphate-buffered saline (PBS; 10 mmol, pH 7.4), Dulbecco's modified Eagle's medium, fetal bovine serum (FBS), and antibiotic-antimycotic solution were purchased from Life Technologies (Gibco, USA). The HT1080, MCF7, MKN45, and HEK293T cell lines were purchased from the American Tissue Type Culture (ATCC, USA). Ultrapure deionized water was used for all syntheses and all other chemicals and reagents were of analytical grade.

2.2. Synthesis of MNCs

The MNC was synthesized using a thermal decomposition method, previously described in [13, 14]. Briefly, in the case of the magnetite nanoparticle (MNP), 2 mmol iron (III) acetylacetonate, 10 mmol 1,2-hexadecanediol, 6 mmol dodecanoic acid, 6 mmol dodecylamine, and 20 mL benzyl ether were mixed in a three-necked flask and magnetically stirred. The mixture was preheated to 100 °C under a nitrogen flow to remove residual O_2 and H_2O for 30 min. The preheated mixture was heated to 200 °C (10 °C min^{-1}) for 2 h with a water-cooled condenser and refluxed at 300 °C for 30 min under a blanket of nitrogen. After the reactants were cooled to room temperature by removing the heat source, the products were purified with excess ethanol. The black material was precipitated and separated by centrifugation (1811 rcf for 10 min). The precipitate was dissolved in 2 mL hexane in the presence of 0.16 mmol lauric acid. Then, centrifugation (1811 rcf for 10 min) was applied to remove any undispersed residue. The dark brown supernatant was purified by adding excess ethanol with ultrasonication and then centrifuged (1811 rcf for 10 min) to remove the solvent. The precipitate was redispersed with 5 mL hexane. Approximately 12 nm MNP was synthesized following the seed-mediated growth [13, 14]. Manganese ferrite nanoparticle (MFNP) was synthesized using the same process with 2 mmol iron(III) acetylacetonate, 1 mmol manganese(II) acetylacetonate, 10 mmol 1,2-hexadecanediol, 6 mmol dodecanoic acid, 6 mmol dodecylamine, and 20 mL benzyl ether.

2.3. Synthesis of mP80

For the preparation of mP80, 22.9 mmol N,N'-Dicyclohexylcarbodiimide and 15.3 mmol MPA were dissolved in respective flasks containing 10 mL dichloromethane and the reagents were subsequently mixed. The mixture was added to 20 mL dichloromethane containing 7.6 mmol P80 and 3.2 mL triethylamine was dispersed into the mixture. Finally, 22.9 mmol 4-(dimethylamino) pyridine was dissolved in 10 mL dichloromethane and all reagents were mixed in a 70 mL vial. The final mixture was magnetically stirred for 48 h. The color of the mixture changed from an apricot to a red wine color. After reacting for 48 h, the crystallized urea was removed by filtration. To eliminate the dichloromethane, the reaction was filtered by evaporation in a rotary evaporator (N-1100, EYELA, Japan). The resulting product was dispersed in deionized water, and the unconjugated reagents were removed by dialysis (Spectra/Por®, 3.5 kDa MWCO, Spectrum Laboratory Inc., USA). The final product was prepared by freeze-drying. The synthesized mP80 was confirmed by comparison with MPA and P80 using a UV–vis spectrometer (2120UV Mecasys, Republic of Korea), and Fourier-transformed infrared spectroscopy (FT-IR, PerkinElmer, spectrum two) using an ^{1}H-NMR spectrometer (JUM-ECP300, JEOL Ltd Japan; figure 2).

2.4. Preparation of maleimidyl MNP and MFNP

Water-soluble maleimidyl MNP (mMNP) was prepared using the nanoemulsion method [13]. In detail, 30 mg MNP was dissolved in 4 mL hexane (as the organic phase) and the organic phase was mixed with 20 mL deionized water (as the aqueous phase) containing 100 mg mP80. After mutual saturation of the organic phase with the aqueous phase, the emulsion was ultrasonicated in an ice-cooled bath for 10 min at 190 W. The organic solvent was evaporated overnight at room temperature and the products were purified using a dialysis membrane (Spectra/Por®, 3.5 kDa MWCO, Spectrum Laboratory Inc., USA). The distribution of the hydrodynamic diameter of the mMNP was analyzed using a

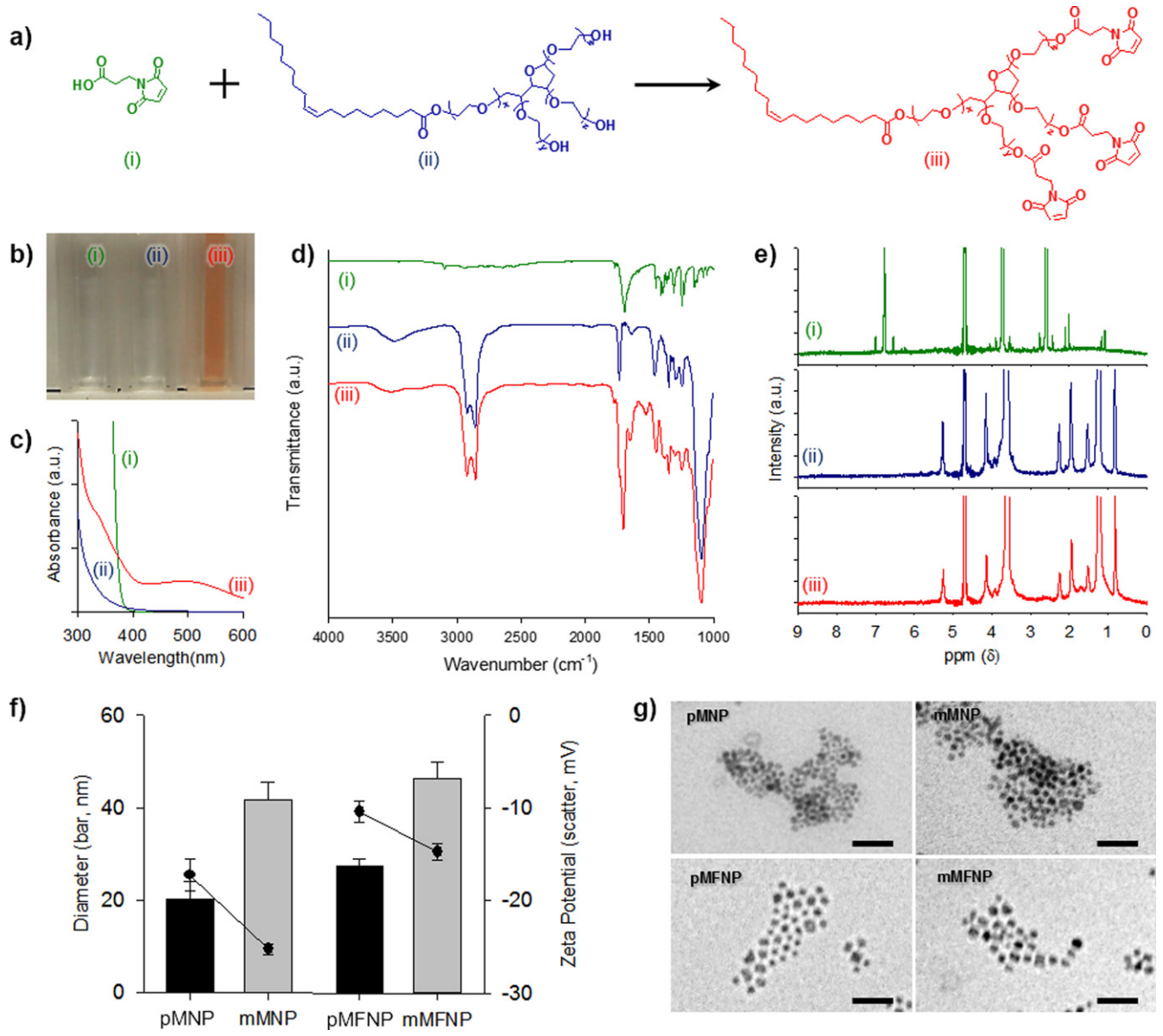

Figure 2. Physicochemical characterization of mP80, mMNP, and mMFNP. (a) Diagram of the synthesis process for mP80: (i) MPA, (ii) P80, and (iii) mP80. (b) Photograph and (c) absorbance spectra of (i), (ii), and (iii) dispersed in deionized water. (d) FT-IR and (e) ^{1}H-NMR spectra of (i), (ii), and (iii). (f) Hydrodynamic diameter and zeta potential and (g) TEM images of pMNP and mMNP (scale bars: 40 nm).

dynamic laser scattering analyzer (ELS-Z, Otsuka Electronics, Japan). The morphology of the mMNP was confirmed using transmission electron microscopy (JEM-1011, JEOL Ltd., Japan). To investigate the ability of the mMNP to act as an MRI contrast agent, MRI experiments were performed at various concentrations of mMNP with a 1.5 tesla clinical MRI instrument with a micro-47 surface coil (Intera, Philips Medical Systems, Netherlands). The T2 relaxivity (R2) of the mMNP was measured at room temperature by the Carr–Purcell–Meiboom–Gill sequence: TR = 10 s, 32 echoes with 12 ms even echo space, number of acquisitions = 1, point resolution = 156 μm × 156 μm, and section thickness = 0.6 mm. R2 was defined as 1/T2 with units of s^{-1}. The relaxivity coefficient ($mM^{-1}\ s^{-1}$) equals the ratio of R2 to the mMNP concentration. The colloidal stability of the mMNP was confirmed against various pH ranges. Maleimidyl MFNP (mMFNP), P80-enveloped MNP (pMNP), and P80-enveloped MFNP (pMFNP) were also synthesized and confirmed by the same method.

2.5. Preparation of biomarker-specific MRI probe

To prepare the biomarker-specific MRI probe, MT1-MMP-specific peptide or EpCAM aptamer was conjugated with mMNP and mMFNP. Briefly, 10 mg mMNP or mMFNP was dissolved in PBS (1 mL), 0.45 nmol peptide or aptamer was added, and the mixture was stirred at room temperature. After 2 h, the mixture was stored at 4 °C, and the peptide-conjugated mMNP and mMFNP and aptamer-conjugated mMFNP were named P-mMNP, P-mMFNP, and A-mMFNP, respectively.

2.6. Analysis of biomarker-expression level

To analyze the biomarker-expression level, quantitative real-time PCR and confocal laser scanning microscopy or western blot were performed. The MT1-MMP gene expression in the HT1080 and MCF7 cell lines was analyzed using quantitative real-time PCR. Total RNA was extracted from the HT1080 and MCF7 cells using the Ambion mirVana™ miRNA Isolation Kit (Cat No. AM1560, Ambion, USA). The total RNA was converted to cDNA using the high capacity RNA-to-cDNA kit (Applied Biosystems, Cat No. 4387406) according to the manufacturer's recommendations. Quantitative real-time PCR (1 μg RNA/sample) was performed using the Roche LightCycler® system (Roche Diagnostics, 20 μL/reaction) for MT1-MMP. The thermocycling conditions were as follows: an initial denaturation step at 95 °C for 10 min, followed by 45 cycles at 95 °C for 10 s and at 60 °C for 30 s (annealing and extension). The primer sequences were designed using the Primer3 software [http:// frodo.wi.mit.edu/primer3/; MT1-MMP primer sequences: (forward) TTG GAC TGT CAG GAA TGA GG and (reverse) GCA GCA CAA AAT TCT CCG TG]. The 2-ΔΔCt method was applied to calculate the fold differences in gene expression using the gene Actin-beta as a housekeeping reference for data normalization. The PCR products were subjected to melting-curve analysis to rule out the synthesis of nonspecific products.

To investigative the expression level of MT1-MMP, confocal laser scanning microscopy was conducted using HT1080 and MCF7 cells treated with FITC-labeled MT1-MMP peptide. Forty micromoles of FITC-labeled MT1-MMP peptide were treated to a concentration of 5.0×10^4 cells/well and the cells were incubated for 30 min Following incubation, the cells were stained using Hoechst 33342 (Invitrogen, USA), for nuclei, and Acti-stain™ 555 Phalloidin (Cytoskeleton Inc. USA), for F-actin, and observed by confocal laser scanning microscopy (LSM 700, Carl Zeiss, Germany).

The expression level of EpCAM in MKN45 and HEK293T cells was determined by flow cytometry. Suspensions of 5.0×10^5 cells were collected, washed three times with blocking buffer [0.2% FBS and 0.02% sodium azide in PBS (pH 7.4)] to prevent nonspecific binding of antibodies, and then incubated with FITC-conjugated antimouse EpCAM (BD Biosciences, USA) for 30 min at 4 °C. The cells were resuspended in 400 μL 4% paraformaldehyde solution and stored at 4 °C prior to flow cytometry. Unbound antibodies were washed off, and the cells were analyzed no later than 1 h after staining on a BD FACScalibur (BD Bioscience, USA).

2.7. In vitro cytotoxicity analysis

The cytotoxicities of pMNP and pMFNP were evaluated using an MTT cell proliferation assay kit I (Roche, Switzerland). The HT1080 or MCF7 cells were seeded into a 96-well plate at a density of 1.0×10^4 cells/well and incubated at 37 °C in a humidified atmosphere with 5% CO_2. Twenty-four hours after incubation, the cells were treated with various concentrations of pMNP or pMFNP for 24 h. Following treatment, the HT1080 and MCF7 cells were washed with 100 μL PBS and transferred to 100 μL fresh 10% Dulbecco's modified Eagle's medium. Subsequently, the cells were treated with the MTT assay solution according to the manufacturer's instructions. Cell viability was evaluated by a microplate reader (Synergy H4 hybrid reader, BioTek) at 584 nm (reference wavelength = 650 nm). All experiments were performed in triplicate. Cell viability was determined from the ratio of the absorbance values for the treated cells to those for the untreated control cells. Cytotoxicity analyses for mMFNP, P-mMFNP (HT1080, MCF7), and A-mMFNP (MKN45, HEK293T) were also performed, respectively.

2.8. Analysis of in vitro targeting ability of biomarker-specific MRI probe

To evaluate the targeting ability of the biomarker-specific MRI probe, dark-field microcopy was conducted using HT1080 and MCF7 cells. The HT1080 and MCF7 cells (2.0×10^4 cells/well) were seeded in four-well plates containing a cover glass and incubated at 37 °C for 24 h. After incubation with P-mMNP or P-mMFNP for 1 h at 37 °C, the cells were washed with PBS and fixed with 4% paraformaldehyde. To determine the binding affinity of P-mMNP or P-mMFNP to the cells, light-scattering images were recorded using an inverted microscope (BX51, Olympus, Japan) with a high numerical aperture dark-field condenser (U-DCW, Olympus, Japan). The targeting ability of A-mMFNP was confirmed by fluorescence dark-field microscopy using the same seeding conditions.

To evaluate the targeted MRI of EpCAM and the detection capacity of A-mMFNP, MKN45 and HEK293T cells (1.0×10^7 cells/tube) were incubated with 3 mL A-mMFNP (0.1 mg mL^{-1}) for 4 h at 37 °C. After washing away the unbound A-mMFNP, the T2 of the collected cells was investigated using a 1.5 T clinical MRI instrument (Philips Medical Systems, Netherlands) with a micro-47 surface coil (Intera; Philips Medical Systems, Netherlands). For T2-weighted MRI, the following parameters were adopted: resolution = 0.234 × 0.234 mm, section thickness = 0.6 mm, TE = 15 ms, TR = 400 ms, and number of acquisitions = 1. Following MRI, the cellular uptake efficiencies of A-mMFNP were quantified by measuring the magnetic ion (Mn and Fe) concentrations of the MRI samples using inductively coupled plasma atomic emission spectroscopy (Thermoelectron Co.). The untreated cells were used as a negative control.

2.9. In vivo MRI

All animal experiments were conducted with the approval of the Association for Assessment and Accreditation of Laboratory Animal Care International. To establish the orthotopic mouse model of gastric cancer, MKN45 cells (1.0×10^7 cells) were implanted into the fundic glands of the stomachs of male mice (six-week-old BALB/c-nude mice). After two weeks, the tumor size was measured using MRI. When the tumor size reached approximately 500 mm^3, water-soluble A-mMFNP was injected intravenously into the tail vein. *In vivo* MRI experiments were performed with a 3.0 T clinical MRI

instrument. For T2-weighted MRI at 3.0 T, the following parameters were adopted: TR = 1054 ms, even echo space, number of acquisitions = 1, point resolution = 400 × 319 mm, section thickness = 0.5 mm, and TE = 70 ms.

2.10. Histological analysis

Following *in vivo* MRI, hematoxylin and eosin (H&E) and Prussian blue staining were conducted to confirm the A-mMFNP targeting of EpCAM-expressing gastric cancer. The tissues were embedded in paraffin after being dehydrated in increasing alcohol concentrations and cleared in xylene. Slices (thickness = 10 μm) were mounted onto glass slides and placed twice in a container filled with hematoxylin for 10 min to stain the nuclei. The tissues were rinsed in water for 10 min to remove the hematoxylin, and the cytoplasm was stained with eosin and dehydrated in the same manner as previously described. After washing the tissue samples three times for 30 min, we added two to three drops of the samples onto the slides and then covered the slides with cover slips.

To visualize the extent of A-mMFNP loading, an additional slide was stained using the Prussian blue staining kit. All stained tissue sections were analyzed using a virtual microscope (Olympus BX51, Japan) and Olyvia software.

3. Results and discussion

For the maleimidylation of P80, the hydroxyl group of P80 was first modified into a maleimidyl group using MPA by an esterification process (figure 2(a)). For confirmation of the P80 modification process, several analyses were carried out. The picture and absorbance spectra of P80, MPA, and mP80, which were soluted in deionized water, are shown in figures 2(b), (c). The spectrum of mP80 was slightly red-shifted before conjugation with MPA; thus, the new absorption peak at 500 nm appeared and the color of mP80 also became a light red. The characteristic band of mP80 was confirmed by FT-IR (figure 2(d)). The carboxyl group (1690 cm^{-1}; figure 2(d),(i)) of MPA reacted with N,N'-Dicyclohexylcarbodiimide to form an O-acyl isourea intermediate, which was more reactive than the free acid. The hydroxyl groups of P80 (3300–3600 cm^{-1}; figure 2(d),(ii)) attacked this intermediate, forming the corresponding ester conjugation (1730 cm^{-1}; figure 2(d),(iii)) in mP80. The C-O stretch (1098 cm^{-1}) of the oxyethylene chains (-OCH2CH2-) on P80 was maintained at the characterization band of mP80 (1112 cm^{-1}; figure 2(d),(iii)) Furthermore, the synthesis of mP80 was investigated by ^{1}H-NMR The characteristic peak of MPA {δ = 2.63, 4 H, [OCO(CH2CH2)N]; figure 2(e),(i)} was found in mP80 {δ = 2.7, 4H, [OCO(CH2CH2)N]; figure 2(e),(iii)} after the esterification reaction, but was not evident in P80 (figure 2(e),(ii)). Collectively, these results demonstrate that P80 was successfully conjugated with MPA. MNP and MFNP were synthesized using a thermal decomposition method and the diameters of MNP and MFNP were grown to approximately 12 nm by seed-mediated growth.

To prepare the water-soluble maleimidyl magnetic nanoplatform, MNP or MFNP was coated with mP80 using a nanoemulsion method [13], and pMNP and pMFNP were also prepared as described in the experimental section. The unconjugated residues were removed by dialysis and the purified mMNP and mMFNP were analyzed by dynamic laser scattering to demonstrate their hydrodynamic diameter and potential (figures 2(f), (g)), revealing no significant differences in diameter (mMNP: 41.74 ± 3.81 nm and mMFNP: 46.42 ± 3.44 nm). In contrast, there was a difference in diameter between pMNP (or pMFNP) and mMNP (or mMFNP) of approximately 20 nm (pMNP: 20.25 ± 3.86 nm and pMFNP: 27.50 ± 1.36 nm). In other words, the diameter increase indicates that mMNP (or mMFNP) was successfully fabricated by combining MNP (or MFNP) and mP80 using the nanoemulsion method.

To prepare the biomarker-specific MRI probe, MT1-MMP peptide and EpCAM aptamer were selected as targeting moieties, because these biomarkers play a key role in cancer metastasis [9–12]. The selected targeting moieties have a thiol functional group or cysteine, and the biomarker-specific MRI probe was synthesized by mixing the targeting moiety and mMNP or mMFNP under the proper pH. Thus, the process of immobilization on mMNP of mMFNP was simple and did not produce any side products.

To evaluate the targeting ability of MT1-MMP peptide-conjugated mMNP and mMFNP (P-mMNP and P-mMFNP), HT1080 and MCF7 cells were selected because of their different MT1-MMP expression levels [15]. First, the expression level of MT1-MMP mRNA was confirmed using quantitative real-time PCR: the HT1080 cells had a 30-fold greater MT1-MMP mRNA expression level than the MCF7 cells (figure 3(a)). In the confocal laser scanning microscopic images, the FITC fluorescence appeared only in the HT1080 cells (figure 3(b)). This result demonstrates that the HT1080 cells have a lot of MT1-MMP, because the FITC-labeled MT1-MMP peptide was specifically targeted to MT1-MMP, while the confocal microscopic images of the HT1080 and MCF7 cells treated with FITC-labeled MT1-MMP peptide were obtained. After 4 h, cellular fluorescence from FITC was detected in the cytoplasm of the incubated HT1080 cells treated with FITC-labeled MT1-MMP peptide. In contrast, neither of the other conditions showed any significant FITC fluorescence signal, even after 4 h of incubation, reflecting the high specificity and sensitivity of the FITC-labeled MT1-MMP peptide for the MT1-MMP-expressing cancer cells.

The cytotoxicity of pMNP and pMFNP in the HT1080 and MCF7 cells was assessed using the MTT assay until two concentrations; the highest concentration, 0.41 μg mL^{-1}, was diluted ten-fold, respectively. Neither the HT1080 cells nor the MCF7 cells were damaged significantly by treatment with the range of pMNP concentrations used in this study.

To precisely examine the targeting event at a microscopic scale, the cellular affinity of P-mMNP was investigated using dark-field microscopy. Dark-field microscopy is a simple, effective, and low-cost technique for confirming the interaction between nanoparticles and cells [16]. While a dark background was seen around both HT1080 and MCF7 cells without P-mMNP and P-mMFNP, numerous vivid and bright white dots

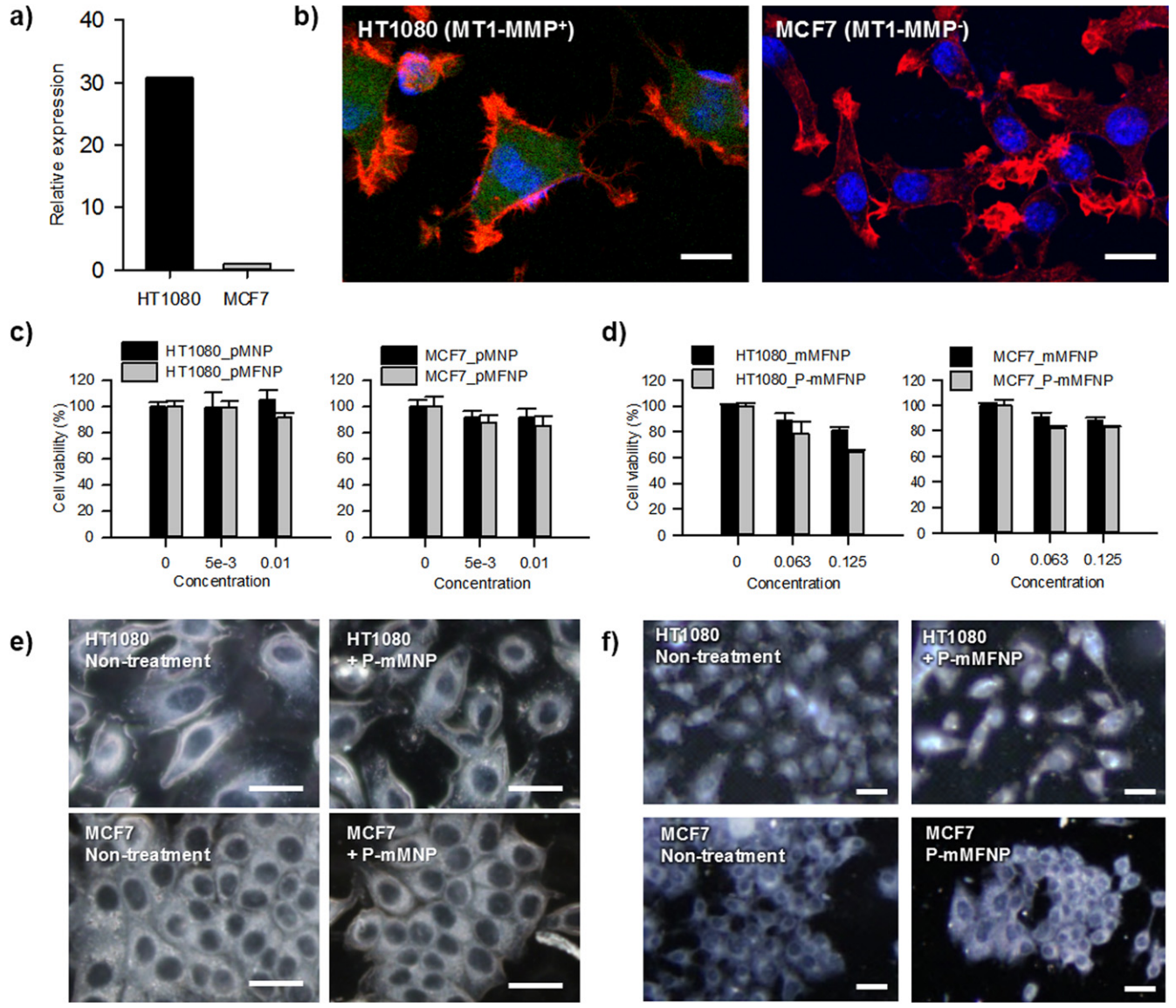

Figure 3. The cell viability and specificity analysis of the peptide-conjugated maleimidyl magnetic nanoplatform (P-mMNP and P-mMFNP). (a) Expression level of MT1-MMP mRNA in HT1080 and MCF7 cells measured by quantitative real-time PCR. (b) Confocal microscopic images of HT1080 and MCF7 cells following treatment with FITC-labeled MT1-MMP. (c) Viability of HT1080 and MCF7 cells treated with different concentrations of pMNP and pMFNP and (d) mMFNP and P-mMFNP. (e) Dark-field microscopic images of HT1080 and MCF7 cells treated with P-mMNP and (f) P-mMFNP (control: nontreatment). All scale bar is 20 μm.

were observed at the outside of the HT 1080 cells. These white dots were caused by the scattering of the incident light by the magnetic nanoparticles (figures 3(e), (f)). The MCF7 cells treated with P-mMNP exhibited no change in appearance compared with the cells that were not treated with P-mMNP, indicating that the P-mMNP specifically bound the MT1-MMP in the HT1080 cell membrane.

To assess EpCAM-targeting cells *in vitro*, the EpCAM-positive MKN45 cells and the EpCAM-negative HEK293T cells were treated with EpCAM antibody and analyzed by flow cytometry (figure 4(a)). The MKN45 cells exhibited EpCAM levels of 99.8% when compared with the HEK293T cells (negative control, 0.3%). The MKN45 and HEK293T cells treated with Hoechst 33342 and EpCAM antibody were analyzed by immunofluorescence microscopy (figure 4(b)). The cells exhibited fluorescence in the nuclei (blue, Hoechst 33342) and in the cytoplasm (green, FITC), confirming the expression of EpCAM in the MKN45 and HEK293T cells. The MKN45 cells were expressed on EpCAM, but the HEK293T cells were not expressed on EpCAM.

To assess the biocompatibility of mMFNP, we investigated the *in vitro* cytotoxicity of A-mMFNP in MKN45 and HEK293T cells by monitoring cell viability and proliferation. The cell viabilities were examined after incubation with various concentrations of A-mMFNP for 24 h. As shown in figure 4(c), the MKN45 and HEK293T cells, each treated with A-mMFNP solution, showed no significant cytotoxicity effects, even at high A-mMFNP concentrations (up to 5.0×10^{-3} mg Fe mL^{-1}). These results indicate that A-mMFNP is biocompatible for use as an MRI probe.

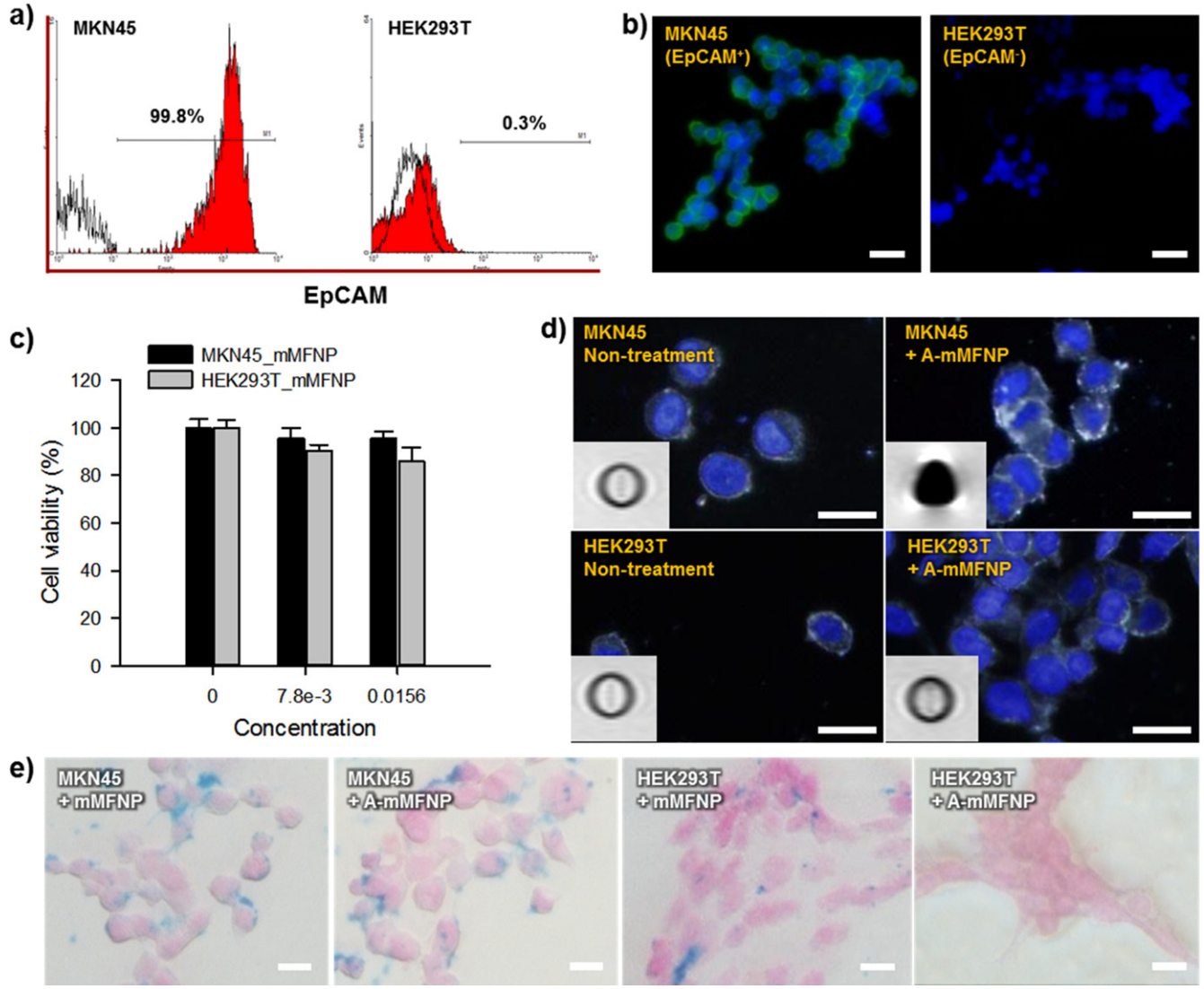

Figure 4. *In vitro* analysis of the EpCAM-targeting ability of EpCAM aptamer-conjugated mMFMP (A-mMFNP). (a) Flow cytometry data and (b) fluorescence microscopic image of MKN45 and HEK293T cells treated with FITC-labeled EpCAM antibody (scale bar: 20 μm). (c) Viability of MKN45 and HEK293T cells treated with different concentrations of A-mMFNP. (d) Dark-field microscopic and cell MRI images of MKN45 and HEK293T cells treated with and without A-mMFNP (scale bar: 10 μm). (e) Microscopic images of MKN45 and HEK293T cells treated with and without A-mMFNP or mMFNP stained by Prussian blue (scale bar: 20 μm).

The cellular binding efficiency of A-mMFNP was investigated using dark-field microscopy. Figure 4(d) shows the scattered spots on MKN45 cells treated with A-mMFNP. However, MKN45 cells that were not treated with A-mMFNP did not express similar spots. These results indicate that A-mMFNP effectively targeted the EpCAM-expressing cells.

The selective accumulation of A-mMFNP within the cells was verified using the Prussian blue staining kit (magnified images). Ferric ions from bound A-mMFNP in the MKN45 cells combined with the ferrocyanide, resulting in the formation of a bright blue pigment called Prussian blue. HEK293T cells treated with A-mMFNP showed red (nuclei) and pink (cytoplasm) pigments, but lacked the blue pigment. These results demonstrate that the cancer cells, which were identified by the *in vitro* MRI, were successfully targeted by the A-mMFNP (figure 4(e)).

To investigate the *in vivo* EpCAM-targeting ability of A-mMFNP using MRI, we prepared the nude-mouse orthotopic xenograft model via the gastric injection of MKN45 cells. MRI of the EpCAM-expressing gastric tumors was obtained after the injection of A-mMFNP into the tail vein of the mice (200 μg Fe) (figure 5(a)). Prior to the administration of both mMFNP solutions (pre-injection), each T2-weighted MRI image of the tumor site appeared characteristically bright, with a low R2 value. Following the injection of A-mMFNP, we observed that the tumor sites showed darkened images caused by the presence of magnetic components. However, the MKN45 tumor sites treated with A-mMFNP were darker than those observed pre-injection, because the A-mMFNP effectively targeted and bound the EpCAM in the tumor tissue. These MRI comparisons between A-mMFNP and mMFNP confirmed that the aptamer effectively targets EpCAM. A-mMFNP enabled precise *in vivo* detection of

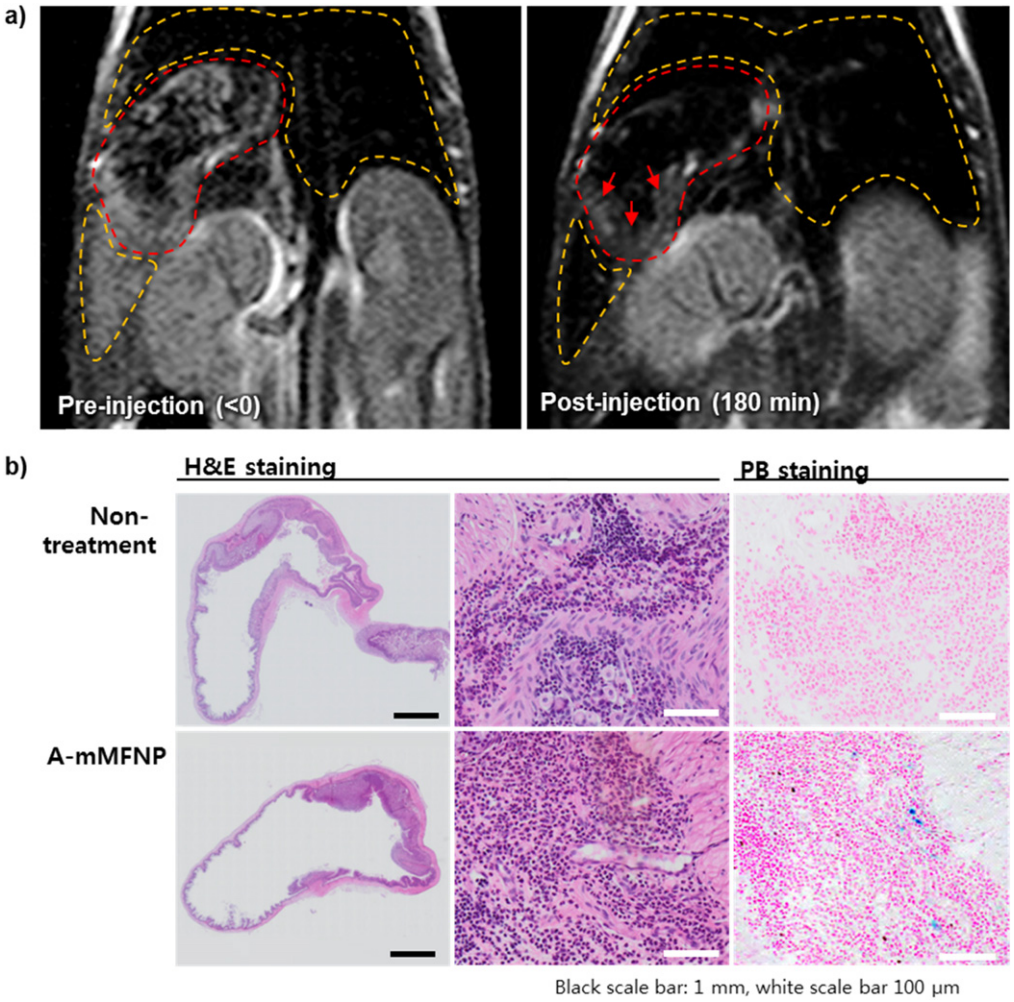

Figure 5. Analysis of the *in vivo* targeting ability of A-mMFNP on gastric cancer. (a) T2-weighted MRI of an EpCAM-expressing gastric cancer orthotopic mouse model after tail vein injection of A-mMFNP. (b) Microscopic images of an H&E-stained and Prussian blue-stained stomach from the EpCAM-expressing gastric cancer orthotopic mouse model following MRI.

EpCAM expressed in the gastric orthotopic xenograft mouse model using MRI.

To determine the precise regions detected by A-mMFNP, histological analysis was performed on the excised gastric tissues following nanoprobe treatment and MRI (figure 5(b)). The dark purple region in the H&E-stained tissues clearly outlines the tumor. The selective accumulation of A-mMFNP within the cells was verified using the Prussian blue staining kit (magnified images). Ferric ions from bound A-mMFNP in the MKN45 tumors combined with the ferrocyanide, resulting in the formation of a bright blue pigment called Prussian blue. The gastric tumors treated with mMFNP showed red (nuclei) and pink (cytoplasm) pigments, but lacked the blue pigment. These results demonstrate that the cancer cells, which were identified by the *in vitro* MRI, were successfully targeted by the A-mMFNP (figure 5(b)).

4. Conclusion

In summary, we developed a maleimidyl magnetic nanoplatform for facile molecular MRI. The fabrication process for targeted MRI probes using the maleimidyl magnetic nanoplatform is simple, efficient, and facilitates the dispersion of MNCs in water and, simultaneously, the conjugation between MNCs and the thiolated targeting moiety without additives and side products. The biocompatibility and targeting ability of the targeted MRI probes based on this platform were confirmed in various *in vitro* and *in vivo* analyses. In particular, the effectiveness of this platform was investigated in two different cancer cell lines using two targeting moieties. Furthermore, although extra purification was not conducted, the absence of significant cytotoxicity and nonspecific binding is especially noteworthy. We believe these results reflect that this platform may be used with molecular MRI to improve the diagnosis of cancer.

Acknowledgements

This work was supported by a National Research Foundation (NRF) grant funded by the Korean government, Ministry of Education and Science Technology (MEST) (2012R1A2A1A01011328), the Industrial Strategic Technology

Development Program (10047677, Development of biocompatible and disease-specific imaging contrast nanomaterials for the guidance of medical treatment by precision tumor detection and high-penetrating imaging) funded by the Ministry of Trade, Industry and Energy (MI, Korea), and a grant from the National R&D Program for Cancer Control, Ministry for Health and Welfare, Republic of Korea (1020390).

References

[1] Louie A Y, Huber M M, Ahrens E T, Rothbacher U, Moats R, Jacobs R E, Fraser S E and Meade T J 2000 *In vivo* visualization of gene expression using magnetic resonance imaging *Nat. Biotech.* **18** 321–5

[2] Weissleder R, Moore A, Mahmood U, Bhorade R, Benveniste H, Chiocca E A and Basilion J P 2000 *In vivo* magnetic resonance imaging of transgene expression *Nat. Med.* **6** 351–4

[3] Lee J-H *et al* 2007 Artificially engineered magnetic nanoparticles for ultra-sensitive molecular imaging *Nat. Med.* **13** 95–9

[4] Weinstein J S, Varallyay C G, Dosa E, Gahramanov S, Hamilton B, Rooney W D, Muldoon L L and Neuwelt E A 2009 Superparamagnetic iron oxide nanoparticles: diagnostic magnetic resonance imaging and potential therapeutic applications in neurooncology and central nervous system inflammatory pathologies, a review *J. Cereb. Blood Flow Metab.* **30** 15–35

[5] Yang J *et al* 2011 Ambidextrous magnetic nanovectors for synchronous gene transfection and labeling of human MSCs *Biomaterials* **32** 6174–82

[6] Winter P M *et al* 2003 Molecular imaging of angiogenesis in early-stage atherosclerosis with $\alpha v\beta 3$-integrin–targeted nanoparticles *Circulation* **108** 2270–4

[7] Massoud T F and Gambhir S S 2003 Molecular imaging in living subjects: seeing fundamental biological processes in a new light *Genes & Development* **17** 545–80

[8] Park J *et al* 2012 Anchored proteinase-targetable optomagnetic nanoprobes for molecular imaging of invasive cancer cells *Angewandte Chemie Int. Ed.* **51** 945–8

[9] Shmelkov S V *et al* 2008 CD133 expression is not restricted to stem cells, and both CD133 + and CD133- metastatic colon cancer cells initiate tumors *J. Clinical Investigation* **118** 2111–20

[10] Mayer B, Johnson J P, Leitl F, Jauch K W, Heiss M M, Schildberg F W, Birchmeier W and Funke I 1993 E-cadherin expression in primary and metastatic gastric cancer: down-regulation correlates with cellular dedifferentiation and glandular disintegration *Cancer Res.* **53** 1690–5

[11] Wolf K, Mazo I, Leung H, Engelke K, Von Andrian U H, Deryugina E I, Strongin A Y, Bröcker E B and Friedl P 2003 Compensation mechanism in tumor cell migration: mesenchymal-amoeboid transition after blocking of pericellular proteolysis *J. Cell Bio.* **160** 267–77

[12] Kajita M, Itoh Y, Chiba T, Mori H, Okada A, Kinoh H and Seiki M 2001 Membrane-type 1 matrix metalloproteinase cleaves CD44 and promotes cell migration *J. Cell Bio.* **153** 893–904

[13] Cho E-J, Yang J, Mohamedali K A, Lim E-K, Kim E-J, Farhangfar C J, Suh J-S, Haam S, Rosenblum M G and Huh Y-M 2011 Sensitive angiogenesis imaging of orthotopic bladder tumors in mice using a selective magnetic resonance imaging contrast agent containing VEGF121/rGel *Investigative Radiology* **46** 441–9

[14] Yang J, Lee C-H, Park J, Seo S, Lim E-K, Song Y J, Suh J-S, Yoon H-G, Huh Y-M and Haam S 2007 Antibody conjugated magnetic PLGA nanoparticles for diagnosis and treatment of breast cancer *J. Mater. Chem.* **17** 2695

[15] Rozanov D V, Deryugina E I, Ratnikov B I, Monosov E Z, Marchenko G N, Quigley J P and Strongin A Y 2001 Mutation analysis of membrane type-1 matrix metalloproteinase (MT1-MMP): The role of the cytoplasmic tail Cys574, the active site Glu 240, and furin cleavage motifs in oligomerization, processing, and self-proteolysis of MT1-MMP expressed in breast carcinoma cells *J. Bio. Chem.* **276** 25705–14

[16] Choi R, Yang J, Choi J, Lim E K, Kim E, Suh J S, Huh Y M and Haam S 2010 Thiolated dextran-coated gold nanorods for photothermal ablation of inflammatory macrophages *Langmuir: ACS J. Surfaces Colloids* **26** 17520–7